SLAC-PUB-10391

Numerical Algorithms for Boundary Problems with Disturbed Axial Symmetry

V. Ivanov
Stanford Linear Accelerator Center

V. Kriklivyy
Design Technological Institute od Digital Techniques, RAS, Russia

Submitted to Nuclear Instrumentation and Methods (NIM) A

Stanford Linear Accelerator Center, Stanford University, Stanford, CA 94309

Work supported by Department of Energy contract DE–AC03–76SF00515.

Numerical algorithms for boundary problems with disturbed axial symmetry

V. Ivanov*
Stanford Linear Accelerator Center, USA
V. Kriklivyy
Design Technological Institute of Digital Techniques, RAS, Russia

June 5, 2003

Abstract

The axial symmetry in the real devices of image electron optics is always disturbed by small defects in manufacturing and assembly. We present a complete method for the numerical simulation of problems with such defects, which includes the algorithms for singularity extraction in a numerical solution of the boundary problem described by the Helmholtz equation. The effective recurrent formulas for evaluation of the kernels of integral representations and their derivatives are constructed. New modification of the well-known Bruns-Bertein [1, 2] method is given, and correlation of this method with an integral equation in variations is investigated. The algorithms are implemented in the codes POISSON-2 [3]-[5] and OPTICS-2 [6]. The results of the numerical simulation for various test problems with different kinds of boundary deformation are given.

PACS: 41.20.Cv; 02.70.Pt; 42.30.Va
Keywords: Electromagnetism; Boundary element method; Electron optics

1 Introduction

Any real device is a three-dimensional one, but most publications on numerical simulation are devoted to two-dimensional problems. It means that a 2D model approximates the real device with adequate accuracy for practice. Nevertheless there are problems where 2D approximations are not sufficient because of high precision requirements. One example of the problems is the design of image-optics devices, which require simulations with so called "optical precision". One of the authors (V. Ivanov [3]) made a special investigation of such requirements, via simulation of varying random error of numerical calculations. He showed that "optical precision" means relative error about 10^{-7} for potential and less accuracy for spatial derivatives of first order (10^{-6}) – fourth order (10^{-3}), for the elements of Gauss optics – 10^{-5}, for aberration coefficients of third order – 0.01, which gives $0.05 - 0.1$ accuracy in spatial and temporal resolution. It is absolutely clear that there are no computer codes to simulate those problems in 3D approximation with the same accuracy. Therefore such problems can be simulated as a set of perturbations of a 2D problem. Thus the defects of manufacturing and assembling of an axisymmetric device can be considered as small perturbations of a 2D model.

There are a lot of publications focus on the study of parasitic aberrations (for example, see [27], [31], [30]), but they did not study how to reach "optical precision" in the field evaluation.

*Correspondence address: 2575 Sand Hill Rd., Menlo Park, CA, 94025, USA. E-mail: ivanov@slac.stanford.edu

Publication [29] concerns the axial perturbation deflecting field functions, but there the field excited with coils. That case there are no field sources in the vicinity of axis, and the beam propagates far from the sources. Another paper [28] focuses on the field disturbances for very specific sector analyzers. Authors of both papers does not provide general algorithm for the evaluation of field disturbances, and did not discuss the accuracy of their numerical calculations. They use simplest shapes of deflectors and sector analyzers when all integrals can be evaluated analytically. In this paper we will pay attention to the most complex case of emission devices of arbitrary shape. This case we should provide high accuracy computations right up to the boundary of domain.

There is an opinion that tolerance problem has more academic value than applied interest , and in electron devices, the assembly tolerances are as good as can be realized. That is not right in principle. We know examples when the yield of good devices in repetition work was about 0.05%. In order to increase this yield you should make your tolerance requirements more strong. But first you should know the most critical requirements for the particular parameters, because you are not able to provide more strong requirements to all parameters of your device.

A stationary electric field with source density ρ is described by the Poisson equation $\Delta\phi = \rho$ for the potential ϕ, which can be represented by the expansion

$$\phi(r, z, \theta) = \Phi(z) + \sum_m \phi_m(r, z) \cos[m(\theta + \theta_m)],$$

where ϕ_m is m-th Fourier harmonic of azimuth expansion for 3D potential in cylindrical coordinates (r, z, θ). There are many publications [8]-[15], where the authors use an integral representation mainly for the harmonics of potential. The most detailed algorithms were described in the books [12] and [13]. Some numerical results were presented in the books [13]-[15]. But all of these publications are incomplete and unsatisfactory in the following missing points:

- no detailed algorithms to evaluate the axial asymptotics for harmonics and their derivatives;
- no algorithms to evaluate the harmonics and their derivatives near the boundary;
- no algorithms to evaluate the edge asymptotics of the boundary contour;
- no algorithms to evaluate the field perturbations in the vicinity of thin two-sided conducting surfaces (fine-structure grid, iris);
- no systematic tests with comparison of analytical and numerical results;
- no results of simulations for practical complex devices with comparisons of numerical and experimental data.

Thus our analysis does not allow us to conclude that the authors of those publications can simulate real devices with appropriate accuracy. Our goal is to present such algorithms and numerical results to complete this picture. Our algorithms can:

1. solve the boundary problems for the potential fields of the following structure
$$\phi(r, z, \theta) = \sum_m \phi_m(r, z) \cos[m(\theta + \theta_m)];$$
2. evaluate the perturbed potential due to deformations of the boundary shape;
3. evaluate the charged-particle trajectories with these perturbations of the potential;
4. solve the inverse problem of electron optics: to find the tolerance for geometry variations of the boundary in a priori defined requirements for image quality parameters.

2 Boundary problems

The potential of the stationary field ϕ is governed by the Poisson equation in a cylindrical coordinate system

$$\frac{1}{r}\frac{\partial}{\partial r}\left(r\frac{\partial\phi}{\partial r}\right)+\frac{\partial^2\phi}{\partial z^2}+\frac{1}{r^2}\frac{\partial^2\phi}{\partial\theta^2}=\rho, \tag{1}$$

and different boundary conditions on the boundary surface $S = S_1 + S_2$. We will show later that Dirichlet

$$\phi|_{S_1} = U(r,z,\theta), \tag{2}$$

and Neumann

$$-\left.\frac{\partial\phi}{\partial n}\right|_{S_2} = E_n(r,z,\theta), \tag{3}$$

boundary conditions with known functions U and E_n produce the boundary integral equations (BIE) of different structures. All other types of boundary conditions produce BIE of similar structures, and we will therefore consider only those conditions on piece-wise smooth parts Γ_1 and Γ_2 of a boundary satisfying the Helder condition.

Expanding the potential and source in the Fourier series on the azimuthal coordinate

$$\phi(r,z,\theta)=\sum_m \phi_m(r,z)\cos[m(\theta+\theta_m)],$$

we obtain the set of the Helmholtz equations for the harmonics

$$\frac{\partial^2\phi_m}{\partial r^2}+\frac{\partial^2\phi_m}{\partial z^2}+\frac{1}{r}\frac{\partial\phi_m}{\partial r}-\frac{m^2}{r^2}\phi_m=\rho_m,\quad m=0,1,2,\ldots,$$

where m is the number of the harmonic, and θ_m is their initial angle.

We assume that the Fourier expansion has fast convergence rate versus m. This is typically true for the following cases:

a) azimuthal dependence of the field is a small perturbation of the axially-symmetric problem;

b) the geometry has planes of symmetry or anti-symmetry (multipole):

$$\phi(r,z,\theta)=\pm\phi(r,z,\theta+\frac{2k\pi}{m}),\quad m\geq 1,\quad k=1,\ldots,m;$$

c) the geometry shape is axially-symmetric, but the boundary conditions have azimuthal dependence, which is proportional to $\cos[m(\theta+\theta_m)]$.

The integral representation of a scalar stationary field with such sources as surface charges σ (corresponding to a single-layer potential), dipoles ν (double-layer potential) on the boundary surface S and volume charge density ρ (volume potential) in V is described by the formula:

$$\begin{aligned}\phi(P) \;=\; & \int_S \sigma(Q)\,G_\sigma(P,Q)\,dS_Q+\int_S \nu(Q)\,G_\nu(P,Q)\,dS_Q+ \\ & \int_V \rho(Q)\,G_\rho(P,Q)\,dV_Q,\end{aligned} \tag{4}$$

where $P=(r,z,\theta)$ - is an observation point, $Q=(r',z',\theta')$ - is a source point, and kernels as Green functions $G_\sigma(P,Q)$, $G_\nu(P,Q)=\partial G_\sigma/\partial\vec{n}_Q$ and $G_\rho\equiv G_\sigma$. Here $\vec{n}_Q$ - is a unit normal vector at the point Q of the boundary surface S; S_Q, V_Q means integration over the coordinates of the source point Q. The kernels and their partial derivatives for the axial symmetry case are [3]

$$\begin{aligned}
G_\sigma(P,Q) &= \frac{r_Q K(t)}{\pi\varepsilon_0\delta}, \quad t=2\frac{\sqrt{r_P r_Q}}{\delta}, \qquad (5)\\
G_\nu(P,Q) &= \frac{G_r\cos(\vec{n}_Q,\vec{e}_r)+G_z\cos(\vec{n}_Q,\vec{e}_z)}{\pi\varepsilon_0\delta},\\
\frac{\partial G}{\partial r}\equiv G_r &= K(t)\left(1+\frac{R_{PQ}^2-4r_Q^2}{2\delta^2}\right)-E(t)\frac{r_P^2-r_Q^2+(z_P-z_Q)^2}{2R_{PQ}^2},\\
\frac{\partial G}{\partial z}\equiv G_z &= E(t)\frac{r_Q(z_Q-z_P)}{R_{PQ}^2}, \qquad (6)\\
\delta &= \sqrt{(r_P+r_Q)^2+(z_P-z_Q)^2}, \quad R_{PQ}=\sqrt{(r_P-r_Q)^2+(z_P-z_Q)^2}.
\end{aligned}$$

Here $K(t)$ and $E(t)$ are complete elliptic integrals of the first and second kind, $\vec{e}_r,\vec{e}_z$ are unit vectors of the coordinate system, $\varepsilon_0=8.86\cdot10^{-12}F/m$ is the permeability of free space.

The Dirichlet condition (2) produces an integral equation for unknown surface charge density

$$\int\limits_S \sigma(Q)\,G_\sigma(P,Q)\,dS_Q = U(P)-\int\limits_V \rho(Q)\,G_\rho(P,Q)\,dV_Q, P\in S_1. \qquad (7)$$

The Neumann condition (3) usually arises on the open parts (holes) of the boundary surface . This condition produces an integral equation

$$\frac{\sigma}{2\varepsilon_0}-\int\limits_S \sigma(Q)\,G_n(P,Q)\,dS_Q = E_n(P)-\int\limits_V \rho(Q)\,G_n(P,Q)\,dV_Q, P\in S_2, \qquad (8)$$

where $G_n(P,Q)=\partial G_\sigma(P,Q)/\partial n_P$.

Taking the Fourier expansion of the boundary condition $f=U$ or $f=E_n$ and for the source σ,

$$f(P) = \sum_m f_m e^{im\theta}, \quad \sigma(Q)=\sum_m \sigma_m e^{im\theta}, \qquad (9)$$

we can obtain the generalized integral equation

$$f_m(P) = \int\sigma_m(Q)\,G_{\sigma,m}(P,Q)d\Gamma_Q+\lambda\sigma_m(P),\ dS_Q\equiv d\theta d\Gamma_Q, \qquad (10)$$

where λ is a constant, Γ is the boundary contour, and the 2D-kernel is now

$$G_{\sigma,m}(r,z;r',z')=r'\int_0^{2\pi}\frac{\cos(m\theta)\,d\theta}{\sqrt{r^2+(r')^2-2rr'\cos\theta+(z-z')^2}}. \qquad (11)$$

Here we use coordinates r,z and r',z' lying on the two-dimensional boundary contour Γ. A similar formula can be written for the double-layer potential

$$f_m(P) = \int\nu_m(Q)\,G_{\nu,m}(P,Q)d\Gamma_Q+\lambda\mu_m(P), \qquad (12)$$

where the kernel is

$$G_{\nu,m}(r,z;r',z')\equiv\frac{\partial G_{\sigma,m}}{\partial n_Q}=r'\int_0^{2\pi}\frac{[(z-z')\sin\beta-(r'-r\,\cos\theta)\cos\beta]\cos(m\theta)\,d\theta}{[r^2+(r')^2-2rr'\cos\theta+(z-z')^2]^{3/2}}, \qquad (13)$$

where β is the angle between the inner normal vector $\vec{n}_Q$ on the boundary and the axis z.

3 Kernel evaluation algorithm

Using analytical integration, the explicit formulas for a few harmonics can be obtained

$$G_{\sigma,0} = \frac{4r'}{\delta}K(t), \tag{14}$$

$$G_{\sigma,1} = \frac{4r'}{\delta t^2}[(2-t^2)K(t) - 2E(t)],$$

$$G_{\sigma,2} = \frac{4r'}{3\delta t^4}[(3t^4 - 16t^2 + 16)K(t) - (8t^2 - 16)E(t)]. \tag{15}$$

As $G_{\sigma,m} \equiv 0$ in $r \to 0$, we introduce a normalized kernel

$$G^*_{\sigma,m} \equiv \left(\frac{r'}{r}\right)^m G_{\sigma,m}(r,z;r',z') \tag{16}$$

instead G_m to exclude the degeneracy of the integral equation near the axis. Later symbol '*' will relate to the normalized (non singular) functions. Then high-order harmonics can be evaluated using the recurrent formula

$$G^*_{\sigma,m+1} = \left(\frac{r'}{r}\right)^{m+1}\left(\frac{1-2m}{1+2m}G^*_{\sigma,m-1} + \frac{4m(2-t^2)}{(1+2m)t^2}G^*_{\sigma,m}\right),\ m \geq 1,\ \alpha \leq t \leq 1. \tag{17}$$

Parameter α is a constant, which characterizes the bound near-axis domain. Similar formulas have been obtained in publications [15, 18, 21, 22], but without analysis of the field behavior near the axis and the boundary.

Near the axis ($0 \leq t \leq \alpha$) in the limit $r \to 0$ we obtain the simpler expressions

$$G^*_{\sigma,m} = \frac{2\pi r'}{\delta}\sum_{n=m}^{\infty}\xi_{nm}t^{2n},\ \xi_{nm} = \left[\frac{(2n-1)!!}{(2n)!!}\right]^2\frac{(n!)^2}{(n+m)!\,(n-m)!}, \tag{18}$$

$$G^*_{\mu,m} = \frac{2\pi}{\delta}\left(\frac{2r'}{\delta}\right)^{2m}\sum_{n=m}^{\infty}\left[(2n+1)\frac{r'}{\delta}\left(\frac{z-z'}{\delta}\sin\beta - \frac{r'}{\delta}\cos\beta\right) - n\cos\beta\right]\xi_{nm}t^{2(n-m)}. \tag{19}$$

The parameter α is determined in order to get good agreement between both methods of kernel evaluation (17) and (18). The relative difference is less then 10^{-8} for $\alpha = 0.2$. Hawkes and Kasper [12] analyze near-axis asymptotics. They claim their algorithms have been well tested, but there were no numerical results presented for their tests and for practical problems. Some results for test problems have been provided in [13], but these authors did not make a normalization procedure, and did not take into account near-axis asymptotics for σ_m. As the result they lose accuracy of calculations for $m \geq 1$.

4 Numerical algorithm for integral equations

The boundary collocation method consists of the following steps. The boundary contour includes a set of $\bar{m}$ smooth lines described by parametric equations with parameter s

$$r = r_i(s),\ z = z_i(s),\ \alpha_i \leq s \leq \beta_i,\ i = 1,\ldots,\bar{m}. \tag{20}$$

Each interval $[\alpha_i, \beta_i]$ is divided into n_i subintervals with points $r_{ij}, z_{ij}, j = 1,\ldots,n_i$. Number of contour points N is the dimension of the global matrix.

Then we use a cubic spline approximation for a regular part $\tilde{\sigma}$ of the BIE solution σ

$$\sigma(s) = \frac{\tilde{\sigma}(s)}{(s-\alpha_i)^u(\beta_i - s)^v}, \tag{21}$$

$$\tilde{\sigma}(s) = M_{j-1}\frac{(s_j - s)^3}{6h_j} + M_j\frac{(s - s_{j-1})^3}{6h_j} + \left(\tilde{\sigma}_{j-1} - M_{j-1}\frac{h_j^2}{6}\right)\frac{s_j - s}{h_j} + \left(\tilde{\sigma}_j - M_j\frac{h_j^2}{6}\right)\frac{s - s_{j-1}}{h_j},\ \tilde{\sigma}_j \equiv \tilde{\sigma}(s_j),\ h_j = s_j - s_{j-1},\ j = 1, ..., N. \tag{22}$$

Here u and v are the order of singularity at the contour edge points. The coefficients M_j of the spline function can be evaluated from the continuity condition for the second derivative of the solution $\tilde{\sigma}$ at the internal points of approximation on the boundary curves [23]. Then we substitute this spline representation into the the integral equations (7,8), and satisfy the boundary conditions at the set of collocation points on the boundary contour. In our case the sets of the approximation and the collocation points s_j are identical. As the result of this procedure we obtain a global matrix $\hat{G}$ of dimension $N \times N$ of the linear system

$$\hat{G}\vec{\sigma} = \vec{F}, \tag{23}$$

where $\vec{F}$ is a vector of the boundary values and $\vec{\sigma}$ is a solution vector.

We use the Gauss quadrature formulas for evaluation of the integrals over the boundary, modified Gaussian elimination procedure to solve the linear system, and a polynomial approximation for the elliptical integrals [20]

$$K(t) = a_i\eta^i - b_i\eta^i \ln\eta,\ E(t) = c_i\eta^i - d_i\eta^i \ln\eta,\ \eta = 1 - t^2 \tag{24}$$

with coefficients a_i, b_i, c_i, d_i.

5 Partial derivatives of the kernels

In solving electron-optical problems using a trajectory model, we need to evaluate first-order partial derivatives $E_r = -\partial\phi/\partial r, E_z = -\partial\phi/\partial z$. In using the aberration theory, following O. Scherzer, we can represent the axial potential with the expansion

$$\phi(r,z) = \Phi(z) - \frac{r^2}{4}\Phi''(z) + \Phi''''(z) - \ldots,\ \Phi(z) \equiv \phi(r,0),\ \Phi^{(i)}(z) \equiv \frac{d^i\Phi}{dz^i}. \tag{25}$$

Thus we should evaluate up to fourth-order derivatives of the potential for the third-order aberration model. In any case, we have to evaluate some partial derivatives of the potential. The first derivative of the kernel for m-th harmonics can be written in the form

$$\frac{\partial G_{\sigma,m}}{\partial d} = \frac{4r'}{(2m-1)!!}\frac{\partial}{\partial d}\left(\frac{A_m E(t) + B_m K(t)}{\delta t^{2m}}\right), \tag{26}$$

where A_m, B_m are polynomials of t, and d is the variable r or z.

By introducing definitions

$$U_m(t) \equiv \frac{dA_m}{dt},\ V_m(t) \equiv \frac{dB_m}{dt},\ D_m \equiv C_m(t)(1-t^2) - B_m(t), \tag{27}$$

we can write the final formula for this derivative

$$\frac{\partial G_{\sigma,m}}{\partial d} = \frac{4r'}{(2m-1)!!\delta t^{2m}}\left\{\frac{1}{t}\frac{\partial t}{\partial d}\left[E(t)\left(A_m(1-2m)+tU_m+C_m+\frac{D_m}{1-t^2}\right)-\right.\right.$$
$$\left.\left.K(t)\left(A_m+(1+2m)B_m-tV_m\right)\right]-\left[A_mE(t)+B_mK(t)\right]\frac{1}{\delta}\frac{\partial \delta}{\partial d}\right\}, \quad (28)$$

and propose the following recurrent formulas for evaluation of the coefficients

$$\begin{aligned}
U_{m+1} &= -(2m-1)^2t^3(4A_{m-1}+tU_{m-1})+4m[(2-t^2)U_m-2tA_m], \quad (29)\\
V_{m+1} &= -(2m-1)^2t^3(4B_{m-1}+tV_{m-1})+4m[(2-t^2)V_m-2tB_m],\\
C_{m+1} &= -(2m-1)^2t^4C_{m-1}+4m(2-t^2)C_m+(2m-1)^2(1+t^2)D_{m-1}+4mD_m,\\
D_{m+1} &= 4mD_m-(2m-1)^2D_{m-1}
\end{aligned}$$

with

$$U_0 = U_1 = V_0 = C_0 = 0,\ C_1 = D_0 = D_1 = 1,\ V_1 = -2t. \quad (30)$$

Thus, we can write derivatives for the first harmonics, for example

$$\frac{\partial G_1}{\partial r} = \frac{4r'}{3\delta^3t^2}\left\{\frac{E(t)}{1-t^2}\frac{\delta^2-2r(r+r')}{2r}+\right. \quad (31)$$
$$\left.E(t)\frac{3\delta^2-2r(r+r')}{2r}+K(t)\left[2(r+r')-\frac{\delta^2(4-t^2)}{2r}\right]\right\},$$
$$\frac{\partial G_1}{\partial z} = \frac{4(z-z')}{3\delta^3T^2}\left[2K(t)-E(t)\left(1+\frac{1}{1-t^2}\right)\right]. \quad (32)$$

6 Improvement of the approach by Bruns-Bertein

Production of any real device is inevitably accompanied by some deviations from its ideal model. Small perturbations of the geometry result in perturbations of the electric or magnetic field, which, in turn, result in deviation of electron-optic parameters. One of the earliest approaches to the problem of perturbation theory has been proposed by H. Bruns. In correspondence with his lemma [1],the perturbation of the potential $\delta\phi$ due to the boundary perturbation $\delta\vec{r}$ satisfies by the relation

$$\delta\phi = -\frac{\partial\phi}{\partial\vec{n}}\Big|_\Gamma(\vec{n}\,\delta\vec{r}), \quad (33)$$

where normal derivative is evaluated on the undisturbed boundary contour Γ.

Bruns applied this correlation to the problems of geophysics with volume sources. Later F. Bertein [2] generalized this lemma to electromagnetism with surface sources - single-layer potential. In using BIE, the solution procedure consists of two steps. First, the undisturbed boundary problem is solved, then the perturbation of the potential is evaluated, using the Bruns lemma as the boundary values on the disturbed part of the boundary. There are some problems in using that lemma when the boundary contour has edges or includes thin, two-sided surfaces with different values for the normal derivative of the potential on both sides.

One of the first practical realizations of that approach has been presented by L. Romaniv [14]. A new approach based on the varying of BIE have been proposed in the book [13], where the authors claim that they overcome the mentioned problems, because their BIE has integrable singularities

in principle. However, they did not discuss the details of such numerical algorithms for specific variation types.

Bruns examined the volume potential with kernel $G_\rho(P,Q)$, which is continuous in the volume. In that case there is no question about the side of the normal derivative. Single-layer potential gives two different values for that derivative satisfied by the relation

$$\left.\frac{\partial\phi}{\partial\vec{n}}\right|_{\Gamma_+} - \left.\frac{\partial\phi}{\partial\vec{n}}\right|_{\Gamma_-} = 4\pi\sigma, \tag{34}$$

where Γ_+ and Γ_- are different sides of the boundary contour.

Bertein used a formal mathematical technique without taking into account this specifics. He assumed that the normal derivative is evaluated from the side of the surface where one would know the potential perturbation. That approach is not correct in presence of a thin, two-sided surface. We propose a modification of the Bruns-Bertein approach, which is free from those problems, and can produce the algorithms which are appropriate for evaluation of the tolerance for electron optic parameters of practical devices.

It is evident that the total difference of the potentials from both sides of the disturbed surface is

$$\Delta\phi \equiv \delta\phi_+ - \delta\phi_- = \left(\left.\frac{\partial\phi}{\partial\vec{n}}\right|_{\Gamma_+} - \left.\frac{\partial\phi}{\partial\vec{n}}\right|_{\Gamma_-}\right)\vec{\delta r} = -4\pi\sigma\delta r. \tag{35}$$

A new feature of our approach is that the double-layer potential with dipole density $\delta\mu = -\sigma\delta r$ can produce this discontinuity of the potential. That way, the total perturbation of the potential $\delta\phi_n$ in normal variation of the boundary contour is given by the formulas

$$\delta\phi_{\nu,n}(P) = \int_\Gamma r_Q\delta\nu(Q)\frac{\partial\hat{G}(P,Q)}{\partial\vec{n}_Q}d\Gamma_Q, \tag{36}$$

$$\delta\phi_{\sigma,n}(P) = \delta r_n(P)\int_\Gamma \sigma(Q)\frac{\partial G(P,Q)}{\partial\vec{n}_P}d\Gamma_Q, \tag{37}$$

$$\delta\phi_n(P) \equiv \delta\phi_{\nu,n}(P) + \delta\phi_{\sigma,n}(P),\ \hat{G} \equiv \frac{G(P,Q)}{r(Q)}. \tag{38}$$

The next important point is that the original Bruns-Bertein approach examined only normal variations δr_n of the boundary contour, but in the electron optic applications it is also important to involve the tangential variations δr_τ, described in a similar way

$$\delta\phi_{\nu,\tau}(P) = \int_\Gamma r_\tau(Q)\delta r_\tau(Q)\sigma(Q)\frac{\partial\hat{G}(P,Q)}{\partial\vec{\tau}_Q}d\Gamma_Q, \tag{39}$$

$$\delta\phi_{\sigma,\tau}(P) = \delta r_\tau(P)\int_\Gamma \sigma(Q)\frac{\partial G(P,Q)}{\partial\vec{\tau}_P}d\Gamma_Q, \tag{40}$$

$$\delta\phi_\tau(P) \equiv \delta\phi_{\nu,\tau}(P) + \delta\phi_{\sigma,\tau}(P), \tag{41}$$

where $\vec{\tau}$ is a tangential vector on the boundary contour.

The third point is that the Bruns-Bertein method did not consider the boundary variations δS, which changes the area (stretching-compressing). Taking these variations into account, we obtain the perturbation of the potential $\delta\phi_s$ as

$$\delta\phi_s(P) = \int_\Gamma \sigma(Q)\delta S(Q)G(P,Q)d\Gamma_Q, \tag{42}$$

$$\delta S(Q) = \frac{\frac{\partial r_Q}{\partial s}\frac{\partial\delta r_Q}{\partial s} + \frac{\partial z_Q}{\partial s}\frac{\partial\delta z_Q}{\partial s}}{\left(\frac{\partial r_Q}{\partial s}\right)^2 + \left(\frac{\partial z_Q}{\partial s}\right)^2}, \tag{43}$$

where $r = r(s), z = z(s)$ are the parametric equations of the boundary, and the total perturbation of the potential is

$$\delta\phi(P) = \delta\phi_n(P) + \delta\phi_\tau(P) + \delta\phi_s(P). \tag{44}$$

This perturbation should be used as the known function in the BIE in variations

$$\int_\Gamma \delta\sigma(Q)G(P,Q)d\Gamma_Q = \delta U(P) + \delta\phi(P). \tag{45}$$

The difference between our approach and the "BIE in variations" from the book [13] is similar to the difference between the Euler and Lagrange approaches in the continuum mechanics.

7 Integral representations for the field perturbations

Now we would examine the basic set of typical types of the boundary variations. Each separate perturbation can be described by a small parameter $\hat{\alpha}_i$, and the total perturbation can be represented by the expansion

$$\phi(r,z,\theta) = \phi(r,z) + \sum_{i=1}^{k} \hat{\alpha}_i \phi_i^{(1)}(r,z,\theta) + \frac{1}{2}\sum_{i,j=1}^{k} \hat{\alpha}_i\hat{\alpha}_j\phi_{ij}^{(2)}(r,z,\theta) + \dots. \tag{46}$$

Here $\phi(r,z)$ is an undisturbed potential, $\phi^{(1)}$ and $\phi^{(2)}$ are the first- and second-order perturbations. Later we will examine the linear perturbations only, so the upper index will be dropped.

General expansion on r for disturbed potential can be written in the form

$$\begin{aligned}
\phi(r,z,\theta) &= \Phi(z) - \frac{r^2}{4}\Phi''(z) + \frac{r^2}{16}\Phi''''(z) + \dots \\
&+ \sum_{i=1}^{k} \hat{\alpha}_i \left[\Phi_{i,0}(z) - \frac{r^2}{4}\Phi''_{i,0}(z) + \dots\right] \\
&+ \sum_{i=1}^{k} \hat{\alpha}_i r\cos\theta \left[\Phi_{i,1}(z) - \frac{r^2}{8}\Phi''_{i,1}(z) + \dots\right] \\
&+ \sum_{i=1}^{k} \hat{\alpha}_i r^2\cos 2\theta \left[\Phi_{i,2}(z) - \frac{r^2}{12}\Phi''_{i,2}(z) + \dots\right] + \dots,
\end{aligned} \tag{47}$$

where $\Phi_{i,0}$ are the zero-order harmonics due to the variations conserving axial symmetry; $\Phi_{i,1}$ are the first-order harmonics due to the shift in the r-axis direction or tilt of the axis of some part of the boundary contour; $\Phi_{i,2}$ are the second-order harmonics due to the elliptical deformation of some part of the boundary contour. It is easy to show that the perturbation functions $\delta\phi_{\nu,n}, \delta\phi_{\nu,\tau}, \delta\phi_{\sigma,n}, \delta\phi_{\sigma,\tau}, \delta\phi_{s,n}$ and $\delta\phi_{s,\tau}$ can be expanded to similar expansions.

We should require the existence of the normal derivative of the perturbed potential on the axis, i.e. $\delta\phi_{\nu,n} < \infty$. This requirement puts some conditions on the form of the boundary variations. We can show that those constraints can be written in the form for double-layer potential

$$\delta\vec{r}_{m,n}(Q) = \epsilon\frac{(r')^m\cos(m\theta)}{a(r',z')}\vec{n}_Q, \tag{48}$$

$$\delta\phi_{m,\mu,n}(P) = \epsilon r^m\cos(m\theta)\phi_m^*(r,z), \tag{49}$$

$$\phi^*(r,z) \equiv -\frac{1}{a(r,z)}\int_\Gamma \sigma_m^*(P,Q)W_m^*(P,Q)d\Gamma_Q, \tag{50}$$

$$\sigma_m^*(P,Q) \equiv \sigma_0(Q)\frac{a(r,z)}{a(r',z')}, \tag{51}$$

$$W_m^*(P,Q) \equiv r'\left(\frac{r'}{r}\right)^m \frac{\partial G_m^*(P,Q)}{\partial \vec{n}_Q}, \tag{52}$$

where ϵ is a small parameter of the boundary perturbation, $a(r,z)$ is some non-singular function not equal to zero on the boundary, σ_0 is a solution of the undisturbed boundary problem, and σ_m^*, W_m^* are the normalized source density and the kernel for m-th harmonics.

For tangential deformation of the boundary contour we have the normalized BIE for the single-layer potential

$$\int_\Gamma \sigma_m^*(Q)W_{m,\sigma,\tau}^*(P,Q)d\Gamma_Q = \frac{1}{r^{m-1}}\frac{\partial \phi_m(P)}{\partial \tau_P} \tag{53}$$

with the non singular kernel

$$W_{m,\sigma,n}^*(P,Q) \equiv r\left(\frac{r'}{r}\right)^m \frac{\partial G_{\sigma,m}(P,Q)}{\partial \tau_P} \tag{54}$$

in $r \to 0, r' \to 0$.

Appropriate double-layer BIE for tangential deformations has the normalized kernel

$$W_{m,\mu,\tau}^*(P,Q) = r'\left(\frac{r'}{r}\right)^m \frac{\partial G_m^*(P,Q)}{\partial \tau_Q}, \tag{55}$$

and tangential deformations should satisfy the conditions

$$\delta\vec{r}_{m,\tau}(P) = \epsilon\frac{r^{m+1}\cos(m\theta)}{b(r,z)}\vec{\tau}(P), \tag{56}$$

$$\delta\vec{r}_{m,\tau}(Q) = \epsilon\frac{(r')^{m+1}\cos(m\theta)}{b(r',z')}\vec{\tau}(Q), \tag{57}$$

where $b(r,z)$ is some non-singular function on the boundary.

The perturbed potential due to the tangential variation of the boundary can be written in the form $\delta\phi_{m,\sigma,\tau} = \epsilon r^m\cos(m\theta)\phi_m^*(r,z)$, where

$$\phi_m^*(r,z) \equiv \frac{1}{b(r,z)}\int_\Gamma \sigma_0(Q)r\frac{\partial G(P,Q)}{\partial \tau_P}d\Gamma_Q. \tag{58}$$

Thus, the BIE in variations

$$\int_\Gamma \delta\sigma_m(Q)G_{\sigma,m}(P,Q)d\Gamma_Q = \epsilon r^m\phi_m^*(P) \tag{59}$$

for the unknown perturbation source $\delta\sigma_m$ has the same kernel as the original BIE for undisturbed source σ_m. It differs from the original equations only with the right-hand part, so after discretization we solve the set of the linear systems with the same matrix and with different right-hand vectors.

In the presence of the edges of the boundary contour the source distribution has the polynomial singularities [3]

$$\sigma_m(s) = \frac{\tilde{\sigma}_m(s)}{(s-s_0)^\kappa},\ \kappa = \frac{\gamma-\pi}{\gamma-2\pi}, \tag{60}$$

where γ is the internal angle in the corner point $s = s_0$. The same asymptotics has the source perturbation $\delta\sigma_m^*$. This asymptotics is included in the kernel $\tilde{W}_m^*(P,Q)$, which is integrable.

We should note that publication [13], as well as all other mentioned publications, did not present numerical results for problems with non smooth boundaries. Despite that, the authors of [13] criticize the Bruns-Bertein approach for its inability to be applied to the boundaries with edges. They did not discuss that problem when stating their version of the BIE in variations.

8 Near-axis asymptotics of harmonics

The analysis we presented before shows that $\phi_m(r,z) \sim r^m$ in $r \to 0$, so the derivatives on z have an asymptotics $\partial^i\phi_m/\partial z^i = r^m C(z)$. Differentiating the normalized kernel

$$G_m^*(r,z) = 2\pi\frac{(2m-1)!!}{(2m)!!}\left(\frac{r'}{\delta}\right)^{2m+1} \tag{61}$$

on z, we can obtain the corresponding kernels for evaluation of $\partial^i\phi_m/\partial z^i$ for $i = 1-4$

$$\frac{\partial G_m^*}{\partial z} = -G_m^*\frac{2m+1}{\delta}\frac{z-z'}{\delta}, \tag{62}$$

$$\frac{\partial^2 G_m^*}{\partial z^2} = -G_m^*\frac{2m+1}{\delta^2}\left[1-(2m+3)\left(\frac{z-z'}{\delta}\right)^2\right], \tag{63}$$

$$\frac{\partial^3 G_m^*}{\partial z^3} = G_m^*\frac{(2m+1)(2m+3)}{\delta^3}\left[3\left(\frac{z-z'}{\delta}\right)-(2m+5)\left(\frac{z-z'}{\delta}\right)^3\right], \tag{64}$$

$$\frac{\partial^4 G_m^*}{\partial z^4} = G_m^*\frac{(2m+1)(2m+3)}{\delta^4}\left[3-6(2m+5)\left(\frac{z-z'}{\delta}\right)^2+\right.$$
$$\left.+(2m+5)(2m+7)\left(\frac{z-z'}{\delta}\right)^4\right]. \tag{65}$$

Numerical experiments show these formulas provide high accuracy for the harmonics and their derivatives for m up to at least 15 when using double precision float point operations.

The kernel derivative on r can be written in the form

$$\frac{\partial G_m}{\partial r} = \frac{\pi}{2}\sum_{i=m}^{\infty} m\xi_{i,m}r^{i-1}\frac{(4r')^{i+1}}{\delta^{2i+1}}. \tag{66}$$

This derivative is identically equal to zero for $m = 0$, but for $m \geq 1$ it is enough to use only the main term for $i = m$. Here $\xi_{m,m} = (2m-1)!!/(m!2^{3m})$. The high-order derivatives are given by the formula

$$\frac{\partial^k G_m^*}{\partial r^k} = \frac{\pi}{2}m(m-1)\ldots(m-k+1)\xi_{m,m}\frac{(4r')^{m+1}}{\delta^{2m+1}}r^{m-k}. \tag{67}$$

It is evident that $\partial^k\phi_m/\partial r^k\Big|_{r\to 0} \equiv 0$ for $k < m$. To obtain an explicit asymptotics, we should normalize the solution of the BIE by introducing $\sigma_m^*(Q) = \sigma_m(Q)/(r')^m$. In that case we have the normalized kernel $W_M^{(k)} \equiv \partial^k G_m/\partial r^k\ (r')^m/r^{m-k}$, which is a regular function that is not equal to zero in $r \to 0$. Then radial derivatives of the potential can be written in the normalized form

$$\frac{\partial^k\phi_m(P)}{\partial r^k} = r^{m-k}\int_\Gamma \sigma_m^*(Q)W_m^{(k)}(P,Q)\ d\Gamma_Q, \tag{68}$$

$$W_m^{(k)} = \pi\xi_{m,m}\left(\frac{2r'}{\delta}\right)^{2m+1}\prod_{i=0}^{k-1}(m-i). \tag{69}$$

Let us compare our kernels for $m = 1, 2$

$$W_1^{(1)} = \pi \left(\frac{r'}{\delta}\right)^3, \; W_2^{(2)} = \frac{3}{2}\pi \left(\frac{r'}{\delta}\right)^5 \tag{70}$$

with the corresponding kernels from the book [13] p.103

$$\frac{\partial G_1}{\partial r} = \pi \frac{r'}{\delta^3}, \; \frac{\partial^2 G_2}{\partial r^2} = \frac{3}{2}\pi \frac{(r')^3}{\delta^5}. \tag{71}$$

The attempt to evaluate the derivatives of the potential using the last formulas results in the formally divergent integrals. The reason for this divergence is that the asymptotic features of the BIE solution are not taking into account.

We emphasize that our formulas for the axial derivatives $\partial^k G_m / \partial r^k$ include as regular terms $\sim (z - z')/\delta$, as non regular ones $\sim 1/\delta$, so the question of their correctness in near-boundary calculations $\delta \to 0$ can arise. That problem is investigated in the next section.

9 Near-boundary asymptotics of harmonics

The most difficult problem is the evaluation of the potential and its derivatives close to the boundary surface. In practical devices some of these surfaces cross the axis, namely the cathode, fine-structure grid and screen. Following the work [16] the boundary contour Γ can be represented by the sum of the "near" axis zones Γ_i and the "far" axis zone Γ_0. As integrals over the "far" zone are regular ones, we will focuse on the "near" zone only. Let us define the "near" zone to be a circular arc of radius R with center on the axis, and the variable of integration is the angle β, which changes from zero on the axis to some value β_0. Then the singular part of the harmonics of the potential over the "near" zone is given by the formulas

$$\Phi_m(z) = a \int_{\Gamma_i} \sigma_m^*(Q) \left(\frac{r'}{\delta}\right)^{2m+1} d\Gamma_Q = a \int_0^{\beta_0} \frac{\sigma_m^*(\beta) R (\sin\beta)^{2m+1} d\beta}{R_0}, \tag{72}$$

where

$$a = 2\pi(2m-1)!!/(2m)!!, \quad R_0 \equiv \left[1 + 2\frac{z}{R}\cos\beta + \left(\frac{z}{R}\right)^2\right]^{m+1/2}.$$

We can expand the source density in the vicinity of the axis

$$\sigma_m^*(\beta) = \sum_i s_i \beta^i, \tag{73}$$

where s_i are the coefficients of this expansion, and represent the singular integral in the form

$$\Phi_m(z) = aR \int_0^{\beta_0} \frac{(\sigma_m^* - s_0)(\sin\beta)^{2m+1} d\beta}{R_0} + aR \int_0^{\beta_0} \frac{s_0 (\sin\beta)^{2m+1} d\beta}{R_0} \equiv \Phi_m^n + \Phi_m^a. \tag{74}$$

Here the first integral is a regular one, as $(\sigma_m^* - s_0) \sim \beta^2$, but the second integral can be evaluated analytically. For $m = 0$ we obtain

$$\Phi_0^a = \frac{h}{|z| + \psi(z)}, \; h \equiv aFs_0, \; F \equiv \frac{2r_0^2}{1 + \cos\beta}, \; \psi \equiv \sqrt{z^2 + F\left(1 - \frac{z}{R}\right)}, \; r_0 \equiv R\sin\beta. \tag{75}$$

For the limit case of a straight line, where $R \to \infty$ we obtain

$$\Phi_0^a = -2\pi\sigma_0(0)\left(|z| - \sqrt{z^2 + r_0^2}\right), \tag{76}$$

which corresponds to a thin charged disk.

The formula for the first derivative of the potential can be obtained by differentiation on z

$$\frac{\partial\Phi_0^a}{\partial z} = -h\frac{\mathrm{sign}(z) + \psi'}{(|z| + \psi)^2},\ \psi' = \frac{z - F/2R}{\psi}. \tag{77}$$

The discontinuity of this derivative in strict correspondence with the theory is

$$\left[\frac{\partial\phi}{\partial n}\right]_\Gamma = -h\frac{\mathrm{sign}(+0) - \mathrm{sign}(-0)}{\psi^2} = -4\pi\sigma(0). \tag{78}$$

The higher derivative can be obtained by similar way

$$\begin{aligned}
\frac{\partial^2\Phi_0^a}{\partial z^2} &= -\frac{h\psi''}{(|z| + \psi)^2} + 2h\frac{\mathrm{sign}(z) + \psi'}{|z| + \psi)^3}, &(79)\\
\frac{\partial^3\Phi_0^a}{\partial z^3} &= -\frac{h\psi'''}{(|z| + \psi)^2} + 6h\psi''\frac{\mathrm{sign}(z) + \psi'}{|z| + \psi)^3} - 6h\frac{[\mathrm{sign}(z) + \psi']^3}{(|z| + \psi)^4}, &(80)\\
\frac{\partial^4\Phi_0^a}{\partial z^4} &= -\frac{h\psi''''}{(|z| + \psi)^2} + 8h\psi'''\frac{\mathrm{sign}(z) + \psi'}{|z| + \psi)^3} - 6h\frac{(\psi'')^2}{(|z| + \psi)^3} - \\
&\quad 36h\psi''\frac{[\mathrm{sign}(z) + \psi']^2}{(|z| + \psi)^4} + 24h\frac{[\mathrm{sign}(z) + \psi']^4}{(|z| + \psi)^5}, &(81)
\end{aligned}$$

where

$$\begin{aligned}
\psi'' &= \frac{\psi^2 - (z - F/2R)^2}{\psi^3}, &(82)\\
\psi''' &= 3\frac{z - F/2R}{\psi^3}\left[\left(\frac{z - F/2R}{\psi}\right)^2 - 1\right], &(83)\\
\psi'''' &= -\frac{3}{\psi^3} + 18\frac{(z - F/2R)^2}{\psi^5} - 15\frac{(z - F/2R)^4}{\psi^7}. &(84)
\end{aligned}$$

It is easy to show, that the discontinuity of the second derivative

$$\left[\frac{\partial^2\Phi_0^a}{\partial z^2}\right]_{z=z_0} = 8\pi\frac{\sigma_0(0)}{R} \tag{85}$$

vanishes in the limit $R \to 0$.

By introducing a new variable $y^2(\beta) = A + B\cos\beta, A = 1 + (z/R)^2, B = 2(z/R)$, we can rewrite the formula for arbitrary harmonics

$$\Phi_m^a = as_0R\int_0^{\beta_0}\frac{(\sin\beta)^{2m+1}d\beta}{(A + B\cos\beta)^{m+1/2}} = \frac{2a}{B}\int_{y_1}^{y_2}\left[1 - \left(\frac{y^2 - A}{B}\right)^2\right]^m\frac{dy}{y^{2m}}, \tag{86}$$

where $y_1 = |1 + z/R|, y_2 = y(\beta_0)$.

The explicit formulas for the first two harmonics are

$$\Phi_1^a = \frac{2as_0R}{3B^3}\left\{\frac{1}{y}\left[y^4 - 6Ay^2 + 3(B^2 - A^2)\right]\right\}_{y_1}^{y_2}, \tag{87}$$

$$\Phi_2^a = \frac{2as_0}{45B^5}\left\{-3y^5 + 20AY^3 - 15(3A^2 - B^2)y + \frac{60A}{y}(B^2 - A^2) + \frac{5}{y^3}(B^2 - A^2)\right\}. \tag{88}$$

The formula for an arbitrary m in $R \to \infty$ is

$$\Phi_m^a(z) = as_0 \int_{|z|}^{\sqrt{z^2+r_0^2}} \frac{(\zeta^2 - z^2)^m d\zeta}{\zeta^{2m}},\ \zeta \equiv r^2 + z^2. \tag{89}$$

In limit $R \to \infty$ we have

$$\Phi_1^a(z) = as_0\left(\frac{2z^2 + r_0^2}{\sqrt{r^2 + z^2}} - 2|z|\right), \quad \Phi_2^a(z) = as_0\left[\frac{8z^4 + 12z^2r_0^2 + 3r_0^4}{3(r^2 + z_0^2)^{3/2}} - \frac{8}{3}|z|\right]. \tag{90}$$

We used only the first term in the expansion (73) before. As $\sigma_m^*(s)$ is an even function of s, the next-order approximation gives

$$\Phi_m(z) = aR\left\{\int_0^{\beta_0} \frac{(\sigma_m^*(\beta) - s_0 - s_2\beta^2)(\sin\beta)^{2m+1}d\beta}{R_0} + s_0\int_0^{\beta_0}\frac{\sin^{2m+1}\beta d\beta}{R_0} + s_2\int_0^{\beta_0}\frac{\beta^2\sin^{2m+1}\beta d\beta}{R_0}\right\}, \tag{91}$$

where $[\sigma_m^*(z)]'' = 2s_2$.

As before, the first integral can be evaluated numerically, and the second one has been examined already, but third integral can not be integrated in elementary functions. This integral can be evaluated analytically using the expansion σ_m^* on the powers $\cos\beta$ as

$$\sigma_m^*(\cos\beta) = \bar{s}_0 + \bar{s}_2\cos\beta + \bar{s}_4\cos^2\beta + \ldots. \tag{92}$$

We can find the coefficients $\bar{s}_i$ of this expansion comparing it with the (73). Finally we obtain $\bar{s}_2 = -2s_2, \bar{s}_0 = s_0 + 2s_2$. Then we can rewrite the third integral in the form

$$\bar{\Phi}_m^a = -\frac{4as_2R}{B}\int_{y_1}^{y_2}\left[1 - \left(\frac{y^2 - A}{B}\right)^2\right]^m \frac{y^2 - A}{By^{2m}}dy. \tag{93}$$

In particular for $m = 0$ and $m = 1$ we obtain

$$\bar{\Phi}_0^a = -\frac{4as_2R}{3B^2}\left[y^3 - 3Ay\right]_{y1}^{y_2}, \tag{94}$$

$$\bar{\Phi}_1^a = \frac{4as_2R}{5B^4}\left[y^5 - 5Ay^3 + (15A^2 - B^2)y + \frac{5A^3 - AB^2}{y}\right]_{y_1}^{y_2}. \tag{95}$$

In the limit $R \to \infty$ we have for $m = 0$, for example, the formula

$$\bar{\Phi}_0^a(z) = -\frac{4}{3}as_2\left[\sqrt{z^2 + r_0^2}(r_0^2 - 2z^2) + 2z^2|z|\right]. \tag{96}$$

We can show, that the quadratic term in (73) gives a correct value for the discontinuity of third derivative on the boundary in $z = 0$

$$\left[\frac{\partial^3 \bar{\Phi}_0^a}{\partial z^3}\right]_\Gamma = 16\pi \left.\frac{\partial^2 \sigma_0(\beta)}{\partial \beta^2}\right|_{\beta=0}. \tag{97}$$

The high-order derivatives $\partial^i \Phi_m / \partial z^i, \partial^i \Phi_m / \partial z^i$ are evaluated by differentiation of the formulas (91),(93). The function $\bar{\sigma}_m \equiv \sigma_m^* - s_0 - s_2\beta^2$ has the following properties

$$\bar{\sigma}_m|_{\beta=0} = 0, \left.\frac{\partial \bar{\sigma}_m}{\partial \beta}\right|_{\beta=0} = 0, \left.\frac{\partial^2 \bar{\sigma}_m}{\partial \beta^2}\right|_{\beta=0} = 0. \tag{98}$$

This means that the derivatives of the first integral in (91) have the regular kernels for $i = 1, 2$, and we should use the next term s_4 in the expansion (73) to increase the accuracy of calculation for the high-order derivatives ($i = 3, 4$).

10 The results of numerical modeling

10.1 Benchmark results

Some approaches to solving the problems of harmonic analysis can be found in the publications of numerous authors [8−15], [18−22] and in our publications [3−7], [16−17]. Here we will demonstrate some numerical results for the test problems and compare them with analytical solutions. We examine how the different factors affect the accuracy of the numerical solution:

1) smoothness of the boundary contour;

2) proximity of the observation point to the boundary;

3) presence of thin two-side surfaces;

4) number m of the Fourier-harmonics;

5) order i of the spatial derivative of the potential.

Test problem 1. Let consider a sphere of a unit radius. The potential distribution is given by the formula

$$\phi(r, z, \theta) = \begin{cases} Ur^m \cos(m\theta), & R < 1; \\ Ur^m \cos(m\theta)/R^{2m+1}, & R \geq 1; \end{cases} \tag{99}$$

where $R^2 = r^2 + z^2$, U is a maximum of a given potential on the sphere. This problem has a solution with a single-layer potential

$$\sigma_m(r, z, \theta) = \frac{2m+1}{4\pi} U r^m \cos m\theta. \tag{100}$$

Because $\Phi(z) \equiv 0$ at the axis, we use a normalized potential

$$\phi_m^*(r, z) \equiv \frac{\phi_m(r, z, \theta)}{r^m \cos m\theta} = \begin{cases} 1, & R < 1; \\ R^{2m+1}, & R \geq 1. \end{cases} \tag{101}$$

All derivatives $\partial^i \Phi_m / \partial z^i \equiv 0$ inside the sphere, and their axial values outside the sphere are given by the formulas

$$\begin{aligned}
\Phi'_m &= -\frac{2m+1}{z^{2m+2}}, \\
\Phi''_m &= \frac{(2m+1)(2m+2)}{z^{2m+3}}, \qquad (102) \\
\Phi'''_m &= -\frac{(2m+1)(2m+2)(2m+3)}{z^{2m+4}}, \qquad (103) \\
\Phi''''_m &= \frac{(2m+1)(2m+2)(2m+3)(2m+4)}{z^{2m+5}}.
\end{aligned}$$

For our calculations we divided the circle of the boundary contour on 10 intervals and we used 6-point Gauss quadratures for evaluation the integrals. All calculations were done with using floating point arithmetic with a 41-bit mantissa. The numerical results are given in the Table 1. Here the first row for each z is the analytical solution, and the second row is the numerical one.

Table 1: Potential distribution and derivatives onto the sphere

m	z	Φ	Φ'	Φ''	Φ'''	Φ''''
	0.8	1.000000000	0.0	0.0	0.0	0.0
0		1.000000000	$2.6 \cdot 10^{-8}$	$3.1 \cdot 10^{-8}$	$-5.0 \cdot 10^{-7}$	$4.2 \cdot 10^{-6}$
	1.2	0.833333333	0.6944444	1.1574074	-2.893518	9.645062
		0.833333333	0.6944444	1.1574074	-2.893521	9.645107
	0.8	1.000000000	0.0	0.0	0.0	0.0
1		1.000000046	$6.3 \cdot 10^{-9}$	$-6.6 \cdot 10^{-8}$	$7.4 \cdot 10^{-6}$	$8.0 \cdot 10^{-5}$
	1.2	0.578703704	-1.4467593	4.8225309	-20.09388	100.4694
		0.578703731	-1.4467593	4.8225297	-20.09376	100.4680
	0.8	1.000000000	0.0	0.0	0.0	0.0
2		0.000000114	$8.6 \cdot 10^{-7}$	$-3.0 \cdot 10^{-6}$	$1.1 \cdot 10^{-5}$	$3.6 \cdot 10^{-4}$
	1.2	0.401877572	-1.6744899	8.3724494	-48.83929	352.5952
		0.401877717	-1.6744908	8.3724601	-48.83971	352.5871
	0.8	1.000000000	0.0	0.0	0.0	0.0
3		0.999999950	$-2.9 \cdot 10^{-6}$	$-1.9 \cdot 10^{-5}$	$-6.1 \cdot 10^{-4}$	$3.8 \cdot 10^{-3}$
	1.2	0.279081647	-1.6279763	10.853175	-80.13988	678.3234
		0.279081602	-1.6279751	10.853156	-80.13950	678.3071
	0.8	1.000000000	0.0	0.0	0.0	0.0
4		0.999989295	$-6.1 \cdot 10^{-4}$	$-1.7 \cdot 10^{-3}$	$4.2 \cdot 10^{-2}$	$8.7 \cdot 10^{-2}$
	1.2	0.193806699	-1.4535502	12.112919	-111.0351	1110.351
		0.193787015	-1.4533172	12.110282	-111.0093	1110.926
	0.8	1.000000000	0.0	0.0	0.0	0.0
5		0.995737579	$-3.6 \cdot 10^{-2}$	$-1.4 \cdot 10^{-1}$	2.1	6.3
	1.2	0.134587986	-1.2337232	12.337232	-133.6533	1559.289
		0.133843579	-1.2232319	12.193889	-131.8781	1507.492

It is not easy to compare our results with [13] p.161, because those authors presented analytical data with big errors $\sim 10^{-3}$, and they give the results for the interval $z \in [0, 0.5]$. So it is not easy to make a conclusion about the accuracy near the boundary, i.e. when $z \to 1$. Moreover they only present the results for $m \leq 3$.

Test problem 2. The solution of above mentioned problem can be obtained with the double-layer potential. The strict solution for the source density is

$$\nu(r,z,\theta) = \frac{2m+1}{2\pi m} U r^m \cos(m\theta). \tag{104}$$

The normal derivative of this solution is a continuous function on the sphere. The numerical results of our simulations for the potential distribution and its derivatives were identical to the results presented in the Table 1.

Test 3. Let us consider the thin disk of radius r_0 with a potential distribution $\phi(r,z,\theta) = U\cos(m\theta)$, where U is a given constant. It is convenient to write the potential in the space in elliptical coordinates $(\bar{\nu},\bar{\xi},\bar{\theta})$ as

$$\phi(\bar{\nu},\bar{\xi},\bar{\theta}) = U P_{mm}(\bar{\nu}) Q_{mm}(j\bar{\xi})\cos(m\bar{\theta}),\ j \equiv \sqrt{-1}, \tag{105}$$

where $P_n m$ and $Q_n m$ are the Legendre functions of first and second order. Their values for $n = m$ are given by formulas

$$P_{mm} = (1-\bar{\nu}^2)^{m/2}, Q_{mm} = \int_0^\infty \frac{\cosh(mx)dx}{[\bar{\xi}+\cosh x\sqrt{\bar{\xi}^2+1}]^m}. \tag{106}$$

The axi-symmetrical solution of this problem is

$$\phi(r,z) = U\left\{1 - \frac{2}{\pi}\arctan\left[\frac{1}{r_0^2}\left(\frac{R^2-r_0^2}{2} + \sqrt{\left(\frac{R^2-r_0^2}{2}\right)^2 + r_0^2 z^2}\right)\right]\right\}, \tag{107}$$

$$\Phi_0(z) = U\left(1 - \frac{2}{\pi}\arctan\mid z\mid\right),\ \sigma_0 = \frac{U}{\pi^2\sqrt{r_0^2-r^2}},\ R^2 = r^2+z^2, \tag{108}$$

and the first harmonics is described by the formulas

$$\phi_1(\bar{\nu},\bar{\xi},\bar{\theta}) = \frac{2U}{\pi}\sqrt{(1-\bar{\nu}^2)(1-\bar{\xi}^2)}\left\{\frac{\pi}{2} - \arctan\bar{\xi} - \frac{\bar{\xi}}{1+r\bar{\xi}^2}\right\}\cos\bar{\theta},$$

$$\Phi_1(z) = U\left(1 - \frac{2}{\pi}\arctan\mid z\mid - \frac{2\mid z\mid}{\pi(1+z^2)}\right),\ \sigma_1(r,\bar{\theta}) = \frac{2Ur\cos\theta}{\pi^2\sqrt{r_0^2-r^2}}. \tag{109}$$

The solution for the second harmonics is given with the formulas

$$\phi_2(\bar{\nu},\bar{\xi},\bar{\theta}) = \frac{2U}{\pi}(1-\bar{\nu}^2)(1-\bar{\xi}^2)\left\{\frac{\pi}{2} - \arctan\bar{\xi} - \frac{\bar{\xi}}{1+\bar{\xi}^2} - \frac{2\bar{\xi}}{3(1+\bar{\xi}^2)^2}\right\}, \tag{110}$$

$$\bar{\xi}^2 = \frac{1}{r_0^2}\left\{\frac{R^2-r_0^2}{2} + \sqrt{\left(\frac{R^2-r_0^2}{2}\right)^2 + r_0^2 z^2}\right\},$$

$$\bar{\nu^2} = \frac{1}{r_0^2}\left\{-\frac{R^2-r_0^2}{2} + \sqrt{\left(\frac{R^2-r_0^2}{2}\right)^2 + r_0^2 z^2}\right\},$$

and the solution of the integral equation (7) for $m = 1, 2$ is given by formulas

$$\sigma_1(r,\bar{\theta}) = \frac{2U}{\pi^2}\frac{r\cos 2\bar{\theta}}{\sqrt{r_0^2-r^2}},\ \sigma_2(r,\bar{\theta}) = \frac{8U}{3\pi^2}\frac{r^2\cos 2\bar{\theta}}{\sqrt{r_0^2-r^2}}. \tag{111}$$

At the axis we have the potential distribution of normalized potential with $U = 1, r_0 = 1$ as

$$\Phi_2^*(z) = 1 - \frac{2}{\pi}\left\{\arctan \mid z \mid - \frac{\mid z \mid}{1+z^2} - \frac{2 \mid z \mid}{(1+z^2)^2}\right\}. \tag{112}$$

For numerical simulation we divided the radius of disk onto 10 intervals. The first row in the Table 2 corresponds to the analytical solution, and the second row to the numerical one.

Table 2: Axial potential and its derivatives for the 2nd harmonics on the disk

z	Φ	Φ'	Φ''	Φ'''	Φ''''
0.0	1.000000	-1.697653	0.000000	1.01859	0.000000
	1.000000	-1.697653	0.000000	1.01859	0.000000
0.2	0.673428	-1.509207	1.741393	6.02790	-35.0339
	0.673427	-1.509215	1.741468	6.02790	-35.0037
0.4	0.412075	-1.087614	2.250236	-0.58196	-25.1513
	0.412073	-1.087614	2.250259	-0.58204	-25.1514
1.0	0.075587	-0.212207	0.636620	-1.90986	5.09296
	0.075586	-0.212205	0.636616	-1.90986	5.09301

Test problem 4. The next examples show the relation between the boundary deformation and the perturbation of the potential. The first example examines the shift of a thin disk for a small value $\hat{\alpha} = \delta z$ along the axis z. This shift produces a perturbation of the potential $\delta\phi(r, z)$, which corresponds to the formation of a dipole-layer of density $\delta\nu = -\hat{\alpha}\sigma$. The value of the perturbation is evaluated by integration over the surface of disk with the kernel $G_{0,\nu}$, where the number of harmonics $m = 0$

$$\delta\phi(P) = \int_S \delta\nu(Q) G_{0,\nu}(P, Q) dS_Q. \tag{113}$$

The axial distribution of the perturbed field is given by the formulas

$$\delta\Phi_0(z) = \frac{2}{\pi}\frac{\mathrm{sign}(z)}{1+z^2},\ \delta\Phi_0'(z) = -\frac{4 \mid z \mid}{\pi(1+z^2)^2}. \tag{114}$$

The numerical results are presented in the Table 3, where upper row corresponds to the analytical solution, and lower row to the numerical solution with the disk partitioned into 10 intervals along the radius.

Test 5. The next type of variation is a tilt of the axis of the disk by a small angle $\delta\hat{\theta}$. First, we write the potential of the non-perturbed field in spherical coordinates

$$\phi(R, \theta, \psi) = U(1 - \frac{2}{\pi}\arctan\xi),\ \xi^2 = \frac{1}{r_0^2}\left[\frac{R^2 - r_0^2}{2} + \sqrt{\left(\frac{R^2 - r_0^2}{2}\right)^2 + (Rr_0\cos\theta)^2}\right]. \tag{115}$$

Then we expand this expression with a small parameter $\hat{\alpha} = \delta\theta$, and we obtain the first harmonics of the perturbed potential

$$\delta\phi_1(r, z, \theta) = \hat{\alpha}\delta\phi_1^*(r, z) r\cos\theta,\ \delta\Phi_1(z) = \frac{\mathrm{sign}(z)}{\pi(1+z^2)^2}. \tag{116}$$

Table 3: Perturbed potential for the shift a disk along the z axis

z	Φ	Φ'	Φ''	Φ'''	Φ''''
0.0	-0.636620	0.000000	1.273240	0.000000	-15.2789
	-0.636627	$1.1 \cdot 10^{-10}$	1.273236	$3.6 \cdot 10^{-9}$	-15.27930
0.2	-0.612134	0.235436	0.996077	-2.507606	-7.63534
	-0.612137	0.235443	0.996018	-2.506040	-7.67365
0.4	-0.548810	0.378490	0.424170	-2.835298	3.43355
	-0.548812	0.378495	0.424167	-2.835330	3.43338
0.6	-0.468103	0.413032	-0.040493	-1.715011	6.41027
	-0.468104	0.413036	-0.040501	-1.715019	6.41043
0.8	-0.388183	0.378715	-0.265562	-0.608287	4.31694
	-0.388183	0.378717	-0.265569	-0.608277	4.31698
1.0	-0.318310	0.318310	-0.318310	0.000000	1.90986
	-0.318310	0.318311	-0.318314	$1.1 \cdot 10^{-5}$	1.90985

Table 4: Perturbation of the potential due to tilt of the disk's axis

z	Φ	Φ'	Φ''	Φ'''	Φ''''
0.0	-0.318310	0.000000	1.273239	0.000000	-22.9183
	-0.318317	$8.2 \cdot 10^{-9}$	1.273244	$4.5 \cdot 10^{-9}$	-22.9183
0.2	-0.294295	0.226381	0.870696	-3.516274	-8.30768
	-0.294297	0.226385	0.870693	-3.515823	-8.32825
0.4	-0.236556	0.326284	0.140640	-3.200767	8.85479
	-0.236556	0.326288	0.140633	-3.200818	8.85526
0.6	-0.172097	0.303700	-0.297745	-1.182223	9.15643
	-0.172096	0.303702	-0.297754	-1.182209	9.15658
0.8	-0.118348	0.230924	-0.387220	0.103030	3.74739
	-0.118348	0.230924	-0.387224	0.103051	3.74735
1.0	-0.079577	0.159155	-0.318310	0.477465	0.47746
	-0.079577	0.159155	-0.318311	0.477467	0.47742

The comparison of the results is presented in the Table 4.

Test 6. Small shift $\hat{\alpha} = \delta x$ of the disk's axis in xy-plane along the coordinate x produces the first harmonics of the perturbed potential

$$\delta\phi(r, z, \theta) = \hat{\alpha}\delta\phi_1^*(r, z)r\cos\theta,\ \ \delta\Phi_1(z) = -\frac{2 \mid z \mid}{\pi(1+z^2)^2}. \tag{117}$$

The analytical and numerical results for 10 intervals of discretization are presented in the Table 5.

Test problem 7. Analogous to the previous test we consider a variation of the disk's radius by a small value $\hat{\alpha} = \delta r$, and we obtain the expression for the perturbed potential as

$$\delta\Phi_0(z) = \frac{2\hat{\alpha} \mid z \mid}{\pi(1+z^2)}. \tag{118}$$

We obtained the same accuracy from the results of numerical simulations as in the above tests.

Table 5: Perturbation of the potential for a transverse shift of the disk's axis

z	Φ	Φ'	Φ''	Φ'''	Φ''''
0.0	0.000000	0.636620	0.000000	-7.639437	0.000000
	$5.7 \cdot 10^{-12}$	0.636625	$-6.9 \cdot 10^{-9}$	-7.639442	$2.8 \cdot 10^{-9}$
0.2	0.117718	0.498038	-1.253803	-3.817669	31.4533
	0.117723	0.498016	-1.253058	-3.837026	31.5915
0.4	0.189245	0.212085	-1.417649	1.716775	18.5223
	0.189249	0.212083	-1.417693	1.716830	18.5268
0.6	0.206516	-0.020247	-0.857506	3.205137	-1.52993
	0.206516	-0.020254	-0.857513	3.205137	-1.53067
0.8	0.189357	-0.132781	-0.304143	2.158471	-6.82006
	0.189359	-0.132788	-0.304133	2.158504	-6.82049
1.0	0.159155	-0.159155	0.000000	0.954930	-4.77465
	0.159156	-0.159159	$1.1 \cdot 10^{-6}$	0.954915	-4.77474

Test problem 8. Our next example is a model of a spherical capacitor. It includes two spheres: external with radius R_k and zero potential, and internal with radius R_c and potential U. This lens based on the spherical capacitor has the best focusing property. Ignatev [24] has obtained an explicit expression for the perturbed field due to shift of the internal sphere from the common centre

$$\phi(r,z,\theta) = \bar{\phi}\,(r,z) + \frac{\hat{\alpha} r R_c R_k U \cos\theta}{(R_k - R_c)(R_k^3 - R_c^3)} \left[1 - \left(\frac{R_c}{R}\right)^3\right]. \tag{119}$$

Elliptical deformation of the external sphere creates the second harmonics

$$\phi(r,z,\theta) = \bar{\phi}\,(r,z) + \frac{\hat{\alpha} r^2 \cos(2\theta) R_c R_k^2 U}{(R_k - R_c)(R_k^5 - R_c^5)} \left[1 - \left(\frac{R_c}{R}\right)^5\right], \tag{120}$$

where $\hat{\alpha}$ is a small parameter of deformation, $R^2 = r^2 + (R_k - z)^2$ and $\bar{\phi}$ is the non-perturbed potential

$$\bar{\phi}\,(r,z) = \frac{R_k R_c U}{R_k - R_c} \left(\frac{1}{R} - \frac{1}{R_k}\right). \tag{121}$$

Thus we have the normalized perturbed potentials

$$\delta\phi_1^*(r,z) = A_1 \left[1 - \left(\frac{R_c}{R}\right)^3\right], A_1 = \frac{R_c R_k U}{(R_k - R_c)(R_k^3 - R_c^3)}, \tag{122}$$

$$\delta\phi_2^*(r,z) = A_2 \left[1 - \left(\frac{R_c}{R}\right)^5\right], A_2 = \frac{R_c R_k U}{(R_k - R_c)(R_k^5 - R_c^5)} \tag{123}$$

and the axial field distributions

$$\delta\Phi_1(z) = A_1 \left[1 - \left(\frac{R_c}{z - R_k}\right)^3\right], \; \delta\Phi_2(z) = A_2 \left[1 - \left(\frac{R_c}{z - R_k}\right)^5\right]. \tag{124}$$

For the numerical calculations we have used a set of parameters $U = 1, R_c = 1, R_k = 3$, and each sphere was divided onto 10 intervals in the meridian cross-section. Our results are presented in the

Table 6: Perturbation of the potential due to shift the axis of the sphere

z	Φ	Φ'	Φ''	Φ'''	Φ''''
3.0	0.000000	0.000000	0.000000	0.000000	0.000000
	$-2.5 \cdot 10^{-9}$	$5.5 \cdot 10^{-14}$	$-6.5 \cdot 10^{-10}$	$2.3 \cdot 10^{-12}$	$-3.6 \cdot 10^{-8}$
3.8	0.00000000	0.00000000	0.00000000	0.00000000	0.00000000
	$-4.8 \cdot 10^{-10}$	$9.5 \cdot 10^{-8}$	$2.0 \cdot 10^{-6}$	$-1.8 \cdot 10^{-5}$	$-2.7 \cdot 10^{-4}$
4.6	0.04360727	0.02640944	-0.0660236	0.2063238	-0.7737141
	0.04360727	0.02640944	-0.0660236	0.2063238	-0.7737142
5.4	0.05351896	0.00521668	-0.0086945	0.0181135	-0.0452837
	0.05351896	0.00521668	-0.0086945	0.0181135	-0.0452837
6.0	0.05555556	0.00213675	-0.0028490	0.0047483	-0.0094967
	0.05555556	0.00213681	-0.0028507	0.0049564	-0.0095430
6.6	0.00000000	0.00000000	0.0000000	0.0000000	0.0000000
	$-3.8 \cdot 10^{-8}$	$1.3 \cdot 10^{-6}$	$3.4 \cdot 10^{-5}$	$3.4 \cdot 10^{-4}$	$-1.7 \cdot 10^{-3}$

Table 7: Perturbation of the potential due to elliptical deformation of the sphere

z	Φ	Φ'	Φ''	Φ'''	Φ''''
3.0	0.000000	0.000000	0.000000	0.000000	0.000000
	$-1.8 \cdot 10^{-9}$	$-9.5 \cdot 10^{-14}$	$-3.0 \cdot 10^{-8}$	$1.3 \cdot 10^{-12}$	$-3.0 \cdot 10^{-7}$
3.8	0.00000000	0.00000000	0.00000000	0.00000000	0.00000000
	$-6.4 \cdot 10^{-9}$	$1.2 \cdot 10^{-9}$	$7.1 \cdot 10^{-6}$	$6.4 \cdot 10^{-5}$	$3.3 \cdot 10^{-4}$
4.6	0.01112211	0.03113720	-0.1556860	0.0909194	-6.0544575
	0.01112211	0.03113720	-0.1556864	0.0909195	-6.0549373
5.4	0.01836151	0.00048652	-0.0012163	0.0035475	-0.0118251
	0.01836151	0.00048655	-0.0012163	0.0035109	-0.0137600
6.0	0.01851852	0.00012754	-0.0002551	0.0005952	-0.0015871
	0.01851864	0.00012344	-0.0002133	0.0006244	-0.0027830
6.6	0.00000000	0.00000000	0.0000000	0.0000000	0.0000000
	$-5.0 \cdot 10^{-8}$	$-6.8 \cdot 10^{-7}$	$1.0 \cdot 10^{-5}$	$1.1 \cdot 10^{-4}$	$1.0 \cdot 10^{-3}$

Table 6. The comparative results for elliptical deformation of the external sphere of the spherical capacitor are presented in the Table 7.

Test problem 9. We suggest a general solution for a perturbed potential for an arbitrary m in the spherical capacitor

$$\phi(r,z,\theta) = \bar{\phi}\,(r,z) + \hat{\alpha} r^m \cos(m\theta)\ \delta\phi_m^*(r,z), \tag{125}$$

$$\delta\phi_m^*(r,z) = A\left[1 - \left(\frac{R_c}{R-R_k}\right)^{2m+1}\right], A = \frac{R_c R_k^m U}{(R_k - R_c)(R_k^{2m+1} - R_c^{2m+1})}. \tag{126}$$

Perturbation of the potential for this variation is given by the formula

$$\delta\Phi_m(z) = A\left[1 - \left(\frac{R_c}{z-R_k}\right)^{2m+1}\right]. \tag{127}$$

The Table 8 contains the analytical and numerical results for harmonics with $m = 3-5$.

Table 8: Potential distribution and derivatives in the spherical capacitor

m	z	Φ	Φ'	Φ''	Φ'''	Φ''''
	4.2	0.004452149	0.01005383	-0.0670255	0.5026917	-4.189097
		0.004452143	0.01005389	-0.0670237	0.5024259	-4.172442
3	4.6	0.005945602	0.00100652	-0.0050326	0.0283083	-0.176927
		0.005945601	0.00100652	-0.0050326	0.0283084	-0.176933
	5.0	0.006127416	0.00016887	-0.0006755	0.0030396	-0.015198
		0.006127415	0.00016887	-0.0006758	0.0030392	-0.015203
	5.4	0.006162198	0.00003927	-0.0001309	0.0004909	-0.002045
		0.006162212	0.00003927	-0.0001929	0.0004289	-0.005363
	4.2	0.001658918	0.00299100	-0.0249250	0.2284789	-2.284789
		0.001658915	0.00299105	-0.0249269	0.2285137	-2.281889
4	4.6	0.002027774	0.00016843	-0.0010527	0.0072374	-0.054280
		0.002027774	0.00016843	-0.0010527	0.0072374	-0.054281
	5.0	0.002053699	0.00001808	-0.0000904	0.0004973	-0.002984
		0.002053698	0.00001808	-0.0000904	0.0004973	-0.002985
	5.4	0.002056939	0.00000292	-0.0000122	0.0000558	-0.000279
		0.002056935	0.00000297	-0.0000473	0.0001152	-0.000027
	4.2	0.000593564	0.00084618	-0.0084618	0.0916695	-1.069477
		0.000593562	0.00084621	-0.0084625	0.0917084	-1.071033
5	4.6	0.000681976	0.00002680	-0.0002010	0.0016334	-0.014292
		0.000681976	0.00002680	-0.0002010	0.0016334	-0.014292
	5.0	0.000685540	0.00000184	-0.0000110	0.0000718	-0.000503
		0.000685540	0.00000184	-0.0000110	0.0000718	-0.000501
	5.4	0.000605830	0.00000021	-0.0000010	0.0000056	-0.000033
		0.000605830	0.00000016	-0.0000021	0.0000028	-0.000637

The analysis of the results for all test problems allow us to make general conclusions. Our algorithms show a high accuracy of computation. This precision is better than $10^{-5}\%$ for a potential, and it decreases by 1.5 times in increasing order of the derivative k for an arbitrary number of harmonics m. The dependence of the precision on the number M is: it does not change for $m = 0-2$, but it decreases by 1.5 times for each $m \geq 3$.

10.2 Practical problems

10.2.1 Electron-optical converter

An electron optical converter with quasi-spherical field described in [24] has rather small aberrations, because its features are close to the ideal model of spherical capacitor. The scheme of this practical device is shown in Fig. 1, and comparative numerical and experimental data are presented in Table 9. All dimensions are normalized by the cathode radius R_c, and potentials are normalized by the accelerating potential U_a. This electron-optical converter of infra-red range consists of the photo-cathode (with radius R_c, potential $\phi_c = 0$), focusing electrode with potential $\phi = 0.166$ and anode assembly with potential $U_a = 1$. This anode assembly consists of the fine-structure spherical grid (shown as a dashed line) and spherical screen positioned at the best focusing area.

The idea of this lens arise in early 70-th. In order to use it as very fast electron shutter authors

Table 9: Numerical and experimental results for quasi-spherical lens

Parameter	Ideal capacitor	Quasi-spherical lens		
		Simulation	Experiment	Error,%
z_{co}	0.666	0.648	0.65	0.3
M	-1.0	-0.878	-0.87	0.9
z_c	1.0	0.950	0.952	0.2
z_g	2.0	1.78	1.8	1.0
E	0.0	-0.06	0.00	12
$\mathbf{D}_{lc}$	-0.5	-1.1	-0.9	20

introduce a diaphragm with aperture hole of 0.05 mm diameter and deflection electrodes. They spent 2.5 years trying to find appropriate parameters experimentally. That device started work properly after our numerical design only. It was found that the tolerance for the diaphragm position is 0.4%. It is impossible in practice to change this critical position on 0.4% and froze all other parameters after pumping and sealing of real device. But it is much easy and less expensive to do it in numerical design. Thus our numerical models has not only pure academic value.

For this particular device the relative errors for the magnification factor **M**, Gauss plane z_g, cross-over z_c, distortion **E** and curvature $\mathbf{D}_{lc}$ aberration coefficients are induced by defects of assembly. The measured distance cathode-grid z_{co} for the experimental prototype was 0.65 instead 0.648 which was used in numerical modeling. This big difference (20% for the curvature coefficient, and 12% for the distortion coefficient) demonstrates precision requirements to the dimension's tolerance.

10.2.2 Tolerance calculations

Our next example examines the dimension's tolerance for the small defects of cathode lens presented in Fig. 2. Non-perturbed axial field distribution and derivatives are shown in Fig. 3, but Figs. 4-7 show perturbed fields for the variation of cathode radius (0th-order harmonics), tilt of the axis for the cathode surface (1st-order), their elliptic deformation (2nd-order). Non perturbed distribution of the potential and 0th to 3th-order harmonics presented in Fig.7.

As an example of application of our method we considered the prototype of this lens as described in [25]. We have used the MTF-functions for the screen and input fiber-optics from that publication to evaluate spatial resolution of this device. The following defects were taken into account:

- $a_1 = \Delta D_c/2$ – change of the cathode diameter;
- $a_2 = \Delta R_c$ – change of the curvature radius of the cathode;
- $a_3 = \Delta r_{a1}$ – change of the radius of the anode hole;
- $a_4 = \Delta r_{a2}$ – change of the outer radius of the anode cone;
- $a_5 = \Delta L_{ca}$ – change of the cathode-anode distance;
- $a_6 = \Delta L_{cs}$ – change of the cathode-screen distance.

The method of calculations for the defects influence was described in details in [26]. According to the work [17] we can investigate the correlation between small defects of the device a_i and image

defocusing $\Delta z = z_0 - z_s$, where z_0 is axial coordinate of the screen surface, and z_s is axial coordinate of the optimal focusing surface. The defocusing parameter is given by the formula

$$\xi = \xi_s + \frac{\Phi_0' \Delta z}{\mathbf{M}^2 \sqrt{e_0 U_a}}, \tag{128}$$

where ξ_s is the parameter corresponding to an optimal focusing, e_0 is the most probable initial energy of the photo-electron, $\mathbf{M}$ is the electron optic magnification, and U_a is the accelerating potential.

For small defects the image defocusing can be represented with a sum

$$\Delta z = \sum_{i=1}^{n} k_i a_i, \; k_i = \left. \frac{\partial \Delta z_i}{\partial a_i} \right|_{a_i = 0}. \tag{129}$$

Numbers k_i can be obtained, for example, by numerical differentiation of the functions $\Delta z_i(a_i)$ evaluated in computer modeling.

We just considered so called "direct problem" of electron optics which investigates the influence of small defects on electron optical parameters of devices, but the inverse problem has a more important practical interest: to find the appropriate values for defects a_i in the pre-defined value for deviation $\xi - \xi_s$. We will examine two cases:

1. If all defects give the same contribution to the image defocusing, then

$$|a_i| \leq \frac{\mathbf{M}^2 (\xi - \xi_s) \sqrt{e_0 U_a}}{n \Phi_0' k_i}. \tag{130}$$

2. If the values a_i are distributed with a normal distribution law, and their contribution to the standard deviation $\sigma(\xi - \xi_s)$ are equivalent, then

$$\sigma(a_i) \leq \frac{M^2 \sigma(\xi - \xi_s) \sqrt{e_0 U_a}}{\sqrt{n} k_i}, \tag{131}$$

where n is a spatial modulation frequency for a sinusoidal test pattern.

The tolerance for a_i are tighter for the first case, but that case about 16% of lenses had over the acceptable limit in manufacturing. Table 10 shows the result of numerical simulation of acceptable defects of electron optic lenses with diameter of cathode $D_k = 18, 25, 40$ and $80mm$ for different acceptable values of spatial resolution N_0: 70, 60 and 50 pair lines per millimeter. The other parameters were: $\epsilon_0 = 0.25\ eV, M = 1, U_a = 12\ kV$, liminal contrast is 0.03.

11 Acknowledgements

Our special thanks go to V. Dolgashev, G. Schussmann and L. Stingelin for assistance with preparation of the manuscript.

References

[1] H. Bruns, Crelles J. fur Math., 81 (1876) 349.

[2] F. Bertein, Ann. de Radioelectricite 2, 7 (1947) 379.

Table 10: Numerical results for tolerant defects a_i, mm

N_0, mm^{-1}	70		60		50						k_i
D_k, mm	18, 25, 40, 80		18, 25, 40, 80		18, 25		40		80		
i	$\|a_i\|$	$\sigma(a_i)$	$\|a_i\|$	$\sigma(a_i)$	$\|a_i\|$	$\sigma(a_i)$	$\|a_i\|$	$\sigma(a_i)$	$\|a_i\|$	$\sigma(a_i)$	
1	0.01	0.03	0.03	0.07	0.05	0.12	0.07	0.2	0.08	0.2	8
2	0.04	0.1	0.1	0.25	0.2	0.45	0.02	0.6	0.17	0.7	2.4
3	0.04	0.1	0.1	0.25	0.2	0.45	0.02	0.6	0.17	0.7	2.4
4	0.007	0.01	0.02	0.04	0.03	0.08	0.03	0.08	0.04	0.1	16
5	0.01	0.03	0.04	0.08	0.06	0.16	0.08	0.2	0.1	0.2	-7
6	0.1	0.24	0.2	0.6	0.4	1.1	0.5	1.4	0.7	0.7	-1

[3] V. Ivanov. CAD methods in physical electronics. In 2 parts. Novosibirsk, Inst. Math. RAS, 1986.

[4] V. Ivanov. Proc. 2nd Int. Conf. on Computations in Electromagnetism. Nottingham, May 13-15, 1994. UK.

[5] V. Ivanov. Proc. 11th IEEE Int. Pulsed Power Conf., Baltimore, Maryland, June 29- July 2, 1997.

[6] V. Ivanov, Y. Kulikov *et al.*, Proc. XV Conf. "High speed photography, photonics and metrology of high-speed processes". Moscow, 26-29 Nov. 1991.

[7] V. Ivanov et al. Proc. XX Int. Congress on High Speed Photography and Photonics. Victoria, Brit. Columbia, Canada.- 21-25 sept., 1992.

[8] E. Kasper, Optik B.46, 3 (1976) 271.

[9] E. Kasper, Optik, B.68, 4 (1984) 341.

[10] E. Munro, H.C. Chu, Optik, B.61, 1 (1982) 1.

[11] D. Janssen, S. Thiem, Optik, B.79, 4 (1988) 154.

[12] P.W. Hawkes, E. Kasper, Principles of Electron Optics. Vol.1. (Academic Press, London,1989).

[13] V.P. Il'in, V.A. Kateshov, Y.V. Kulikov, M.A. Monastyrski, Numerical methods of optimization of emission electron optic systems, Moscow, Nauka, 1987.

[14] L. E. Romaniv, Approximate solving the Dirichlet problem for Laplace equations in the domains with small disturbances of axial symmentry, PhD thesis, Lvov, 1975.

[15] L. E. Tsyrlin, Selected problems of computation of electric and magnetic fields, Nauka, Leningrad, (1977) 319.

[16] V. Ivanov, Y.V. Kulikov, M.A. Monastyrski, in: New methods of design of electron optic systems, Moscow, Nauka, (1983) 187.

[17] V. Ivanov, A.N. Ignatev, Y.V. Kulikov et al., Optiko- mekhanitcheskaya promyslennost, 3 (1983) 7.

[18] P.L. Kapitza, V.A. Fok, L.A. Vanstein, Zh. Tech. Fis., 29, 10 (1959) 1178.

[19] A.G. Vlasov, I.P. Shakhmatova, Zh. Tech. Fis., 32, 6 (1962) 695.

[20] S.M. Belonosov. In: Vychislitelnye Systemy, Novosibirsk, Computing Center, 12(1964) 5.

[21] B.E. Bonstedt, L.E. Tsyrlin, In: Voprosy Matematicheskoy Fiziki, Leningrad, Nauka (1977) 106.

[22] O.M. Vovk, O.Y. Popov, Zh. Tech. Fis., 44, 11 (1974) 2428.

[23] J.H. Alberg, E.N. Nilson, J.L. Walsh, The Theory of Splines and Their Applications, Academic Press, 1967.

[24] A.N. Ignatev, B.E. Dashevsky, V. Ivanov, Y.V. Kulikov, Optiko-mekhanicheskaya Promyslennost, 11 (1979) 41.

[25] I.P. Crosba, Appl. Optics, 16, 10(1977) 2647.

[26] Y. Kulikov, Radiotekh. Elektron., 17, 2(1972) 374.

[27] M.I. Yavor, A.S. Berdnikov, Nucl. Instrum. and Meth. A363(1995)416.

[28] M.I. Yavor, Adv. Imaging and Electron Physics 86(1993)225.

[29] H. Liu, X. Zhu, E. Munro, J. Vac. Sci. Technol. B8(1990)1676.

[30] H. Liu, X. Zhu, E. Munro, Microelectronic Engineering 41/42(1998)163.

[31] O.L. Krivanek, Ultramicroscopy 55(1994)419.

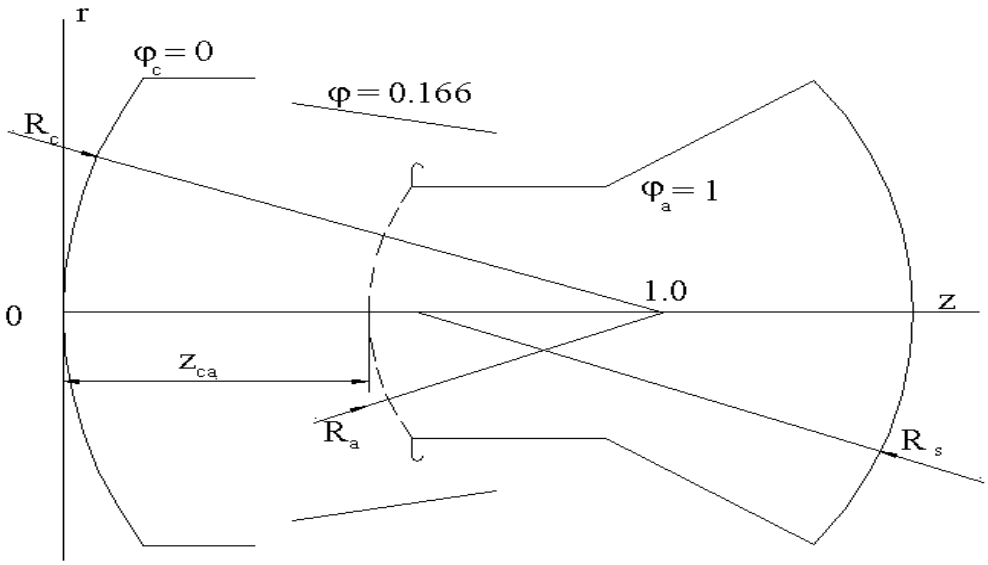

Fig.1. The lens with quasi-spherical field.

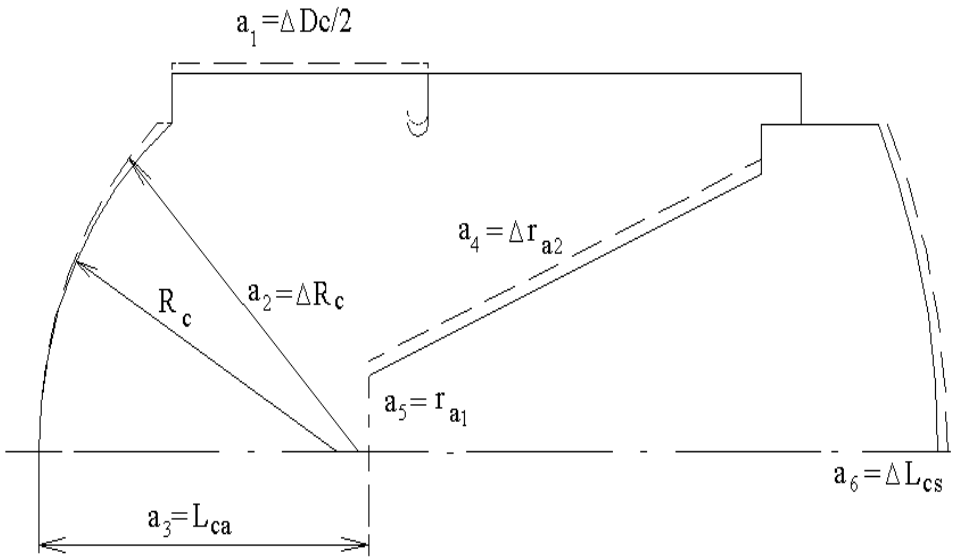

Fig.2. Boundary variations a_i for the electron optic device.

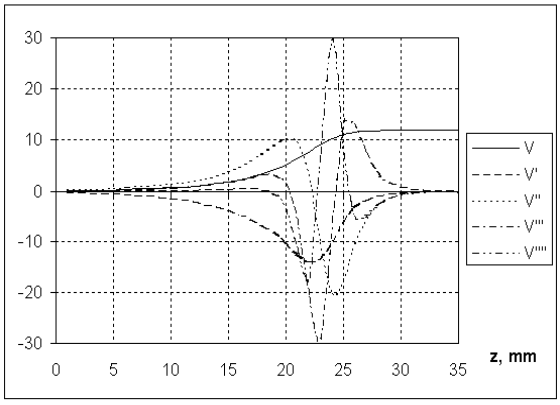

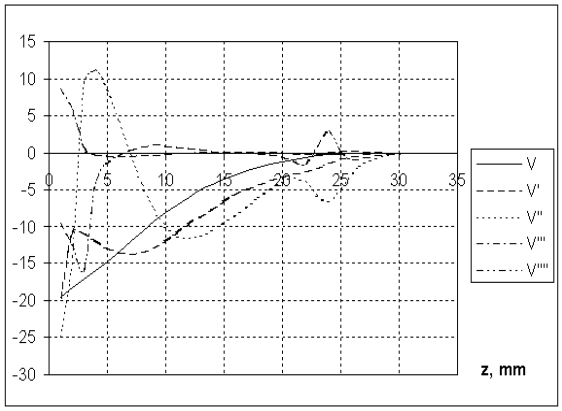

Fig.3. Undisturbed potential and its derivatives; Fig.4 Variation of the cathode radius.

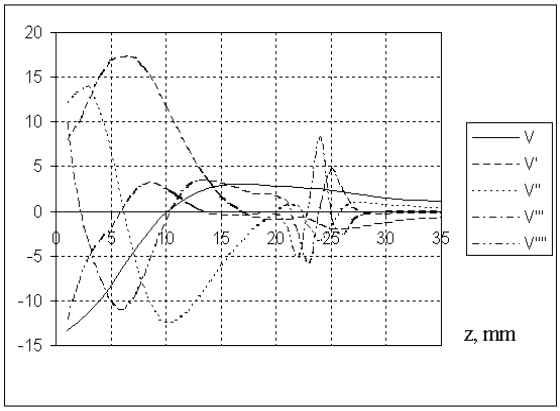

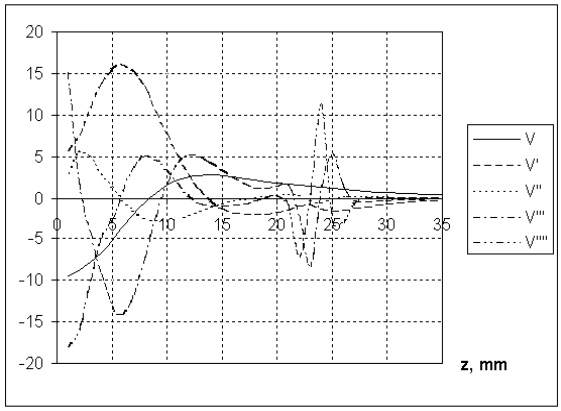

Fig.5. Perturbed field for a tilt of the axis; Fig. 6. Elliptic deformation of the cathode sphere.

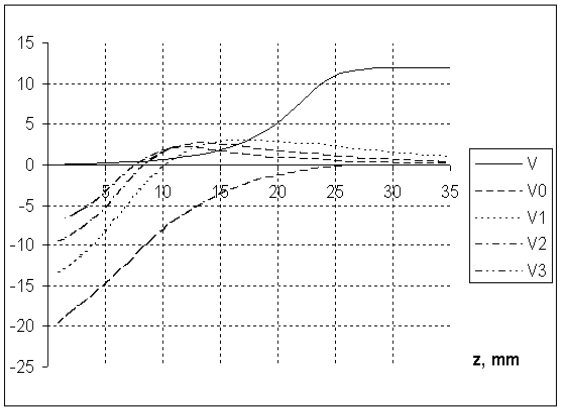

Fig.7. Non-perturbed field V and harmonics V_m for $m = 0 - 3$.